Micropatterning of Quantum Dots for Biofunctionalization and Nanoimaging

Paul Robineau, Jérémie Béal, Thomas Pons, Rodolphe Jaffiol, Cyrille Vézy

Micropatterning of Quantum Dots for Biofunctionalization and Nano-Imaging

Paul Robineau,[†] Jérémie Béal,[†] Thomas Pons,[‡] Rodolphe Jaffiol,[†] and Cyrille Vézy[*,†]

[†]*Light, nanomaterials, nanotechnologies (L2n, CNRS EMR 7004), University of Technology of Troyes (UTT), 12 Rue Marie Curie, 10004, Troyes Cedex, France*

[‡]*Laboratoire de Physique et d'Étude des Matériaux (LPEM, CNRS UMR 8213), ESPCI Paris, Université PSL, Sorbonne Université, 75005 Paris, France*

E-mail: cyrille.vezy@utt.fr

Abstract

Micron-scale patterning of colloidal quantum dots (QDs) is extremely important for the fabrication of high performance Quantum dot Light-Emitting Diode (QLED) displays, bio-sensing and super-resolution imaging. Thus, several non destructive methods have been recently proposed, such as spatial self organization. However none of them can be useful for bio-functionalization or nano-imaging. To address this limitation, we propose a method to create micropatterns of QDs of any shape and any size. UV photolithography assisted by a digital micro-mirror device (DMD) and silanization allow to create an adhesive layer, on which QDs micropatterns can be assembled with a 2 micrometer resolution. The patterns are composed of a monolayer of CdSe/CdS/CdZnS/ZnS core/multishell QDs (7 +/- 1 nm in diameter, emitting at 590 nm) with a high surface density (typically 4000 QDs/μm^2). We also demonstrate that it is possible to reversibly bind any kind of his-tag proteins on the QDs surface. This is

highlighted by measuring FRET (Förster Resonance Energy Transfer) with dedicated polymer exhibiting on one end Alexa Fluor 647 (AF647) and on the other end eight imidazole cycles allowing chelation on the quantum dots surface. Therefore, this patterning protocol provides a path to combine nano-imaging with cell patterning through a relevant biofunctionalization.

Keywords

Quantum dots, Micropatterning, FRET, Super-resolution, Biofunctionalization, Photopatterning

Introduction

Colloidal quantum dots of semi-conductor nanocrystals (QDs) have been developped to exhibit narrow emission spectra, and tunable photostable emission by changing their size and composition.[1–3] They are used in a wide variety of applications such as biosensing,[4–6] integrated photonics,[7,8] light emitting diodes[9,10] or fluorescence imaging.[11,12] In microscopy, QDs are mostly used as fluorescent probes in replacement of usual organic dye molecules. Several years ago we have introduced Nonradiative Excitation Fluorescence Imaging (NEFI),[13] which involves QDs beyond their usual use in fluorescence labeling. This technique is based on Förster Resonance Energy Transfer (FRET) between a surface coated with a monolayer of QDs and fluorescent probes present in the sample. An axial nanoscale resolution can be achieved, allowing outstanding observation on vesicles or living cells.[11] Besides NEFI, several different optical tools have been developed to study cells and their interaction with various substrates. For example, 3d-RICN (Reflection Interference Contrast Nanoscopy) was developed in order to reconstruct lamellipodia in 3D with a nanometric axial resolution. STED (Stimulated Emission Depletion) was used to study inactive or active integrins in sub-diffracted focal adhesion plaques.[14] va-TIRF (variable angle Total Internal Reflection

Fluorescence) is a powerful tool to measure the height of the membrane and to quantify the binding energy in cell adhesion.[15] iPALM (interferometric PhotoActivated Localization Microscopy) was used to map the nanoscale protein organization in focal adhesions.[16] MIET (Metal Induced Energy Transfer) was employed to study the spreading and adhesion of blood platelets.[17] Compared to all this techniques, NEFI provides (as any FRET related techniques) the selectivity required to probe protein-protein interactions on living cells with: (i) no photodamage as in STED; (ii) no long cumulative data recording as with single molecule techniques; and (iii) no complex data processing as in 3d-RICN.

In vivo, cells are located in a highly structured microenvironment. This imposes strong and specific boundary conditions making cells sensitive to various 3D geometrical and mechanical constraints. For instance, the stiffness of the 3D microenvironment will impact cell adhesion and migration by transforming mechanical stress into intracellular signaling pathways.[18] 3D cell culture appears to be the best platform to study biological phenomenoms related to normal or pathological situations. But super-resolution techniques are difficult to use in physiological 3D environment. To overcome this contradiction, it is crucial to micropattern substrates to reproduce *in vivo* cell microenvironment characteristics[19,20] when working in 2D. This patterning will induce modifications and reorganization of actin and microtubule networks and then influence cell adhesion, migration or differentiation. Hence, we decided to create QDs micropatterns on glass substrates, to control cell polarity and the cytoskeletal organization. The QDs micropatterning would indeed play a dual role: (i) as a FRET donor and (ii) as a scaffold for the adhesive proteins (fibronectins, laminins, RGD peptide) which are specifically recognized by cell membrane receptors. Through QDs biofunctionalization, the protein pattern would reproduce the QDs pattern and the cell cytoskeleton architecture can be controlled as well.

Various approaches of QDs patterning have been proposed in the literature using different methods like PDMS flow cell channels,[21] light-driven ligand crosslinking,[22–24] photolithogra-

phy,[25–28] photoresist contact patterning,[29] transfer or microcontact printing,[30,31] inkjet[32] or electrodynamic jet printing,[10,33] liquid transfer approach[34] or the association of Electronic Beam Lithography (EBL) with Langmuir Blodgett film deposition[35] and free direct EBL.[36] Most of these techniques are developed for the field of high performance QLEDs (Quantum dot Light-Emitting Diode) films and rarely for biofunctionalization purposes. Furthermore, none of them can combine a dense QDs monolayer covalently attached on a surface with a free pattern choice. Also the opportunity to graft specifically peptides or proteins through chelation was never done before on micropattern surfaces. The use of chelation for the grafting strategy is pertinent for different reasons. First, chelation induce a specific binding between a metallic cation and histidin or imidazole (the complexant part of histidin). Secondly, hist-tag modified proteins or imidazole block peptide can be easily synthetised. And, chelation is highly specific and reversible. For instance, Dieleman *et al*[27] used UV and EBL to pattern quantum dots with feature sizes of tens of nanometers, but they did not obtain a dense monolayer. Yang *et al*[24] used a light-driven ligand crosslinking, but they needed a physical mask and they also obtained multilayers, with simple designs (only lines or circles) and alkyl ligands are mandatory. In addition, when a QDs monolayer can be obtained from the previous cited techniques, the surface of the QDs monolayer cannot be chemically modify.

In this work, we present a method to produce various micropattern shapes, of highly concentrated QDs monolayers, on a large scale. We have synthezised a fluorescent probe that exhibit 8 imidazole molecules on one side. This imidazole-tag allows specific binding on the QDs surface through chelation between imidazole and zinc present on the QDs shell. We then prove that this binding is specific, reversible and well suited for NEFI experiments. Finally, we demonstrate that our approach is relevant for biofunctionalization and cell nano-imaging on patterns and by recording FRET signal coming from the stained cell membrane.

Results and discussion

QDs micropatterning

Figure 1 describes our QDs photo-patterning method. For that, we have hijacked the primary goal of the Alvéole's PRIMO setup[37] dedicated to protein micropatterning. The UV source (excitation wavelength at $\lambda = 375$ nm) combined with a digital micro-mirror device (DMD) allows for the creation of micropatterns through the illumination of a glass coverslip previously coated with a S1813 G2 positive photoresist layer.

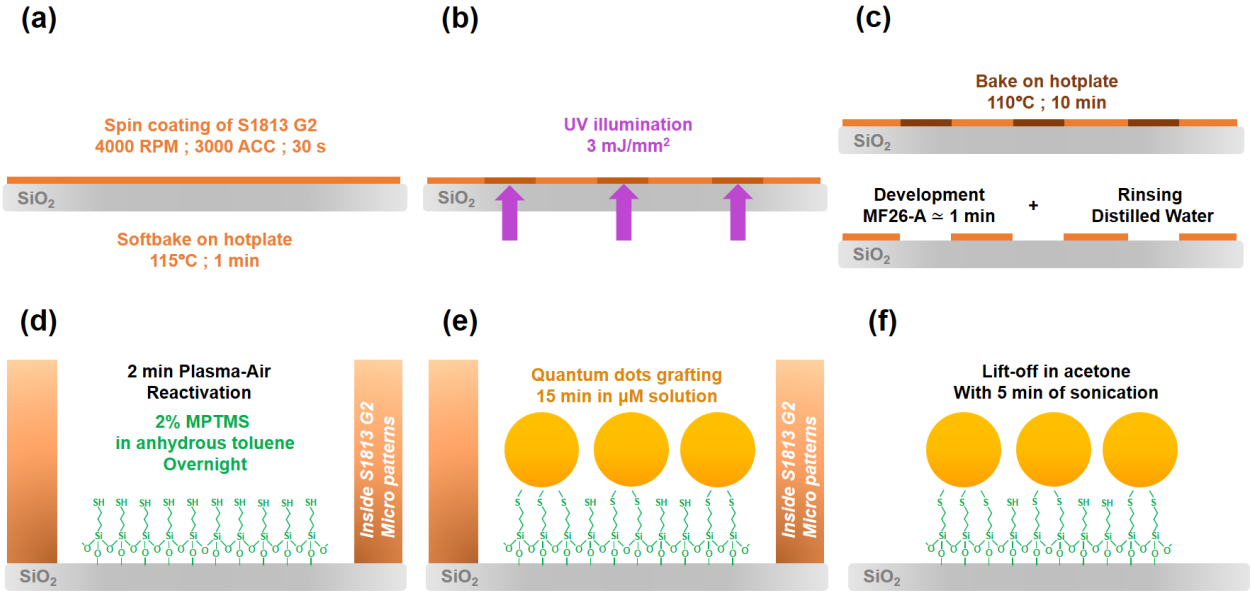

Figure 1: Schematic illustration of our QDs (CdSe/CdS/CdZnS/ZnS core/multishell) micropatterning method on glass coverslips. (a) Spin coating of a thin layer of S1813 G2. (b) UV illumination of the patterns. (c) Soft bake at 110 °C and development step to remove the S1813 G2 previously exposed. (d) Plasma air surface activation and silanization process. (e) QDs grafting through disulfuric bridges between the MPTMS and the ZnS localized at the surface of the QDs. (f) Lift off of S1813 G2 in acetone.

First, the S1813 G2 was exposed with the desired patterns. After the S1813 G2 development, the surface is chemically modified with a silanization process,[11] creating an adhesion layer on which QDs grafting happens through the formation of disulphuric bridges. This method allows to obtain a monolayer. Finally, the obtained surfaces are rinced in acetone to remove the undeveloped S1813 G2. Detailed procedure to prepare the QDs monolayer

patterns is given in the Methods section. High surface densities of QDs monolayer can be reached, as shown on Figure 2 (a), where we estimated a surface density of $\approx$ 4000 QDs/μm^2 with SEM. This high surface density coverage leads to a homogeneous signal of photoluminescence within a diffraction limited spot in microscopy (with a diameter of 0.25 μm), typically $\approx$ 200 QDs . This amount of QDs allows to obtain no blinking from the surface. This is crucial for later FRET analysis as FRET signal fluctuations must come only from distance changes and not from QDs blinking. Figure S1 features the relationship between photoluminescence of the patterns and QDs surface density. The QDs density was performed on several homogenous samples (at least 7) and at different SEM magnification by counting QDs by hands. The density deviation is only $\approx$ 5%. This low deviation in the density conducts to an uniformity in the photoluminescence. This was also ckecked by recording the QDs photoluminescence on 70 different areas of 50 x 50 μm^2. The deviation obtained for the photoluminescence is between 4 and 9 %. As shown on Figure 2 (b)-(h), the use of a DMD means that any kind of shapes can be achieved from circles, squares, stars, simple lines, drops, *etc.*

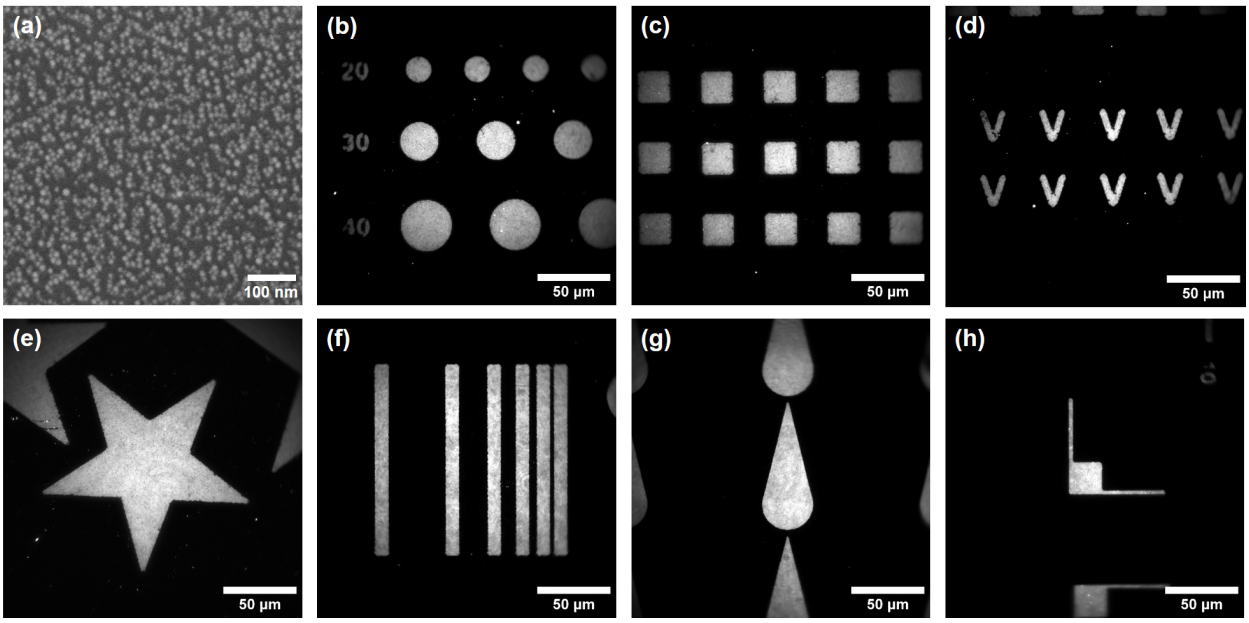

Figure 2: (a) SEM picture of a QDs monolayer on coverglass. From (b) to (h), TIRF images (excitation at λ = 458 nm) of various QDs patterns. All pictures exhibit a surface density of $\approx$ 4000 QDs/μm^2.

We used a decreasing width line pattern to estimate the smallest size that can be obtain and therefore the lateral resolution of our patterning method (Figure 3 (a)). The smallest QDs line that can be created with our technique is around 2 μm (Figure 3 (b)) which corresponds to the optical lateral resolution of the PRIMO system with a 10× objective. Patterning of a 4,62×2,87 mm^2 surface is realized in less than a minute. A (x-y)motorized stage enables to reproduce the micropattern over a large scale. The patterning reproducibility was checked by measuring the integrated radial intensity profile on circle patterns. All profiles overlaped very well and the lateral deviation measured is around 2 µm, which corresponds to our resolution.

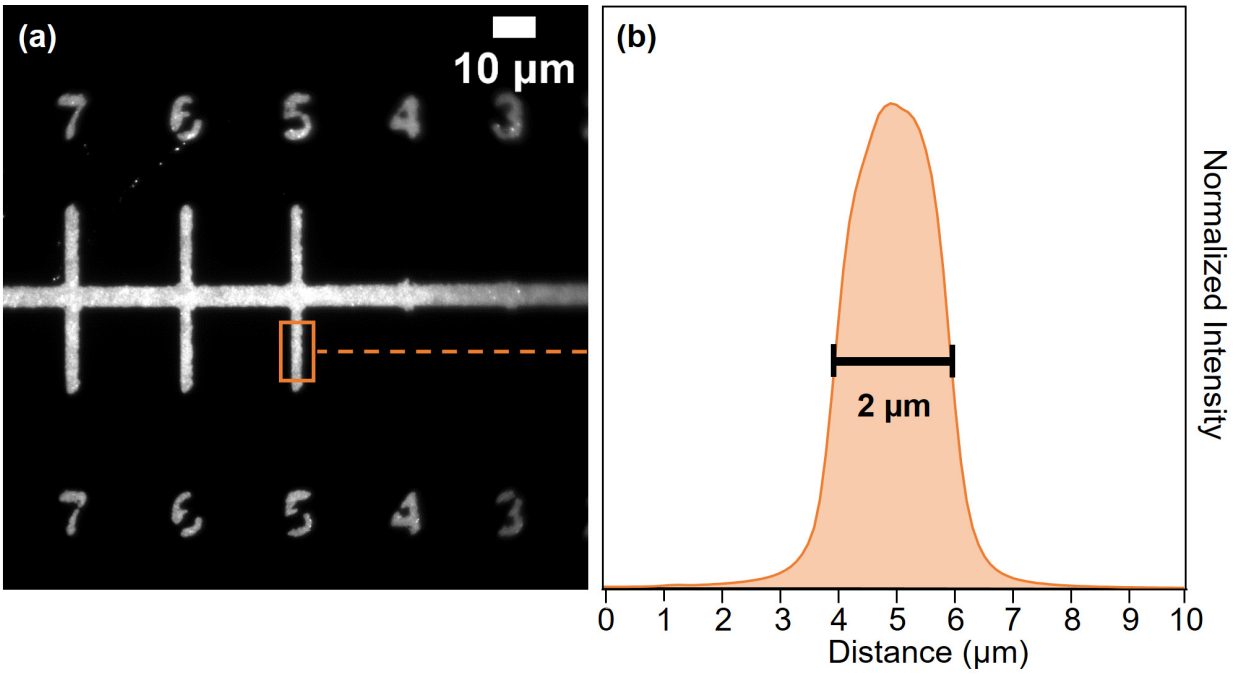

Figure 3: (a) TIRF image of the width decreased lines pattern (excitation at $\lambda = 458$ nm). The numbers indicated the lateral size in pixel of the lines. The smallest line obtained is for 2,5 μm (5 pixels). (b) Averaged photoluminescence profile of the orange zone in (a). The width at half maximum is about 2 μm.

FRET in solution

We firstly demonstrate that (i) specific adhesion of acceptor molecules through chelation process is achieved on our QDs and (ii) the fluorescence recorded from the acceptors in FRET measurements comes from non-radiative excitation process. These first experiments performed in solution will give information about the donor/acceptor ratio achievable in NEFI. To this end,we have developed a small polymer chain that exhibits on one end 8 imidazole cycles to provide chelation on the QDs shells, and on the other end an Alexa fluor 647 molecule. This polymer played the role of the acceptor in FRET. Indeed, poly(imidazole) have been shown to enable strong anchoring of block polymers at the surface of ZnS-terminated QDs, by chelating surface Zn atoms.[38,39] Between the imidazole and the Alexa fluor 647, a block of 26 sulfobetaines was added for the water solubility and for reducing non specific adhesion. The distance from the QD surface to the acceptor dye therefore ranges between 3 nm (gyration diameter of the free polymer chain in solution[40]) and 5.5 nm (fully extended conformation.This polymer will be named pAlexa thereafter. A scheme of the pAlexa structure is given in Figure S2.

We have recorded spectra of different dilutions in water for: (i) pAlexa (acceptor), and (ii) various concentration ratios of QDs:pAlexa. The QDs concentration is kept constant at 50 nM. The photoluminescence emission of QDs is between 550 nm and 640 nm while the fluorescence of the pAlexa is between 640 nm and 770 nm. For an excitation wavelength $\lambda =$ 458 nm, there is no fluorescence emission of pAlexa in the range of 50 nM to 1μM, as shown in Figure 4a. This means that there is no direct excitation of the acceptor at $\lambda = 458$ nm. Due to the narrow emission spectrum of the QDs, donor signal bleed-through in the 640-770 nm spectral window can also be neglected here. Thus, the fluorescence signal recorded in the spectral window of the pAlexa emission is only due to FRET.

When the concentration ratio is fixed at 1:1, we observed a small quenching of the donor photoluminescence and, at the same time, the appearance of fluorescence emission from

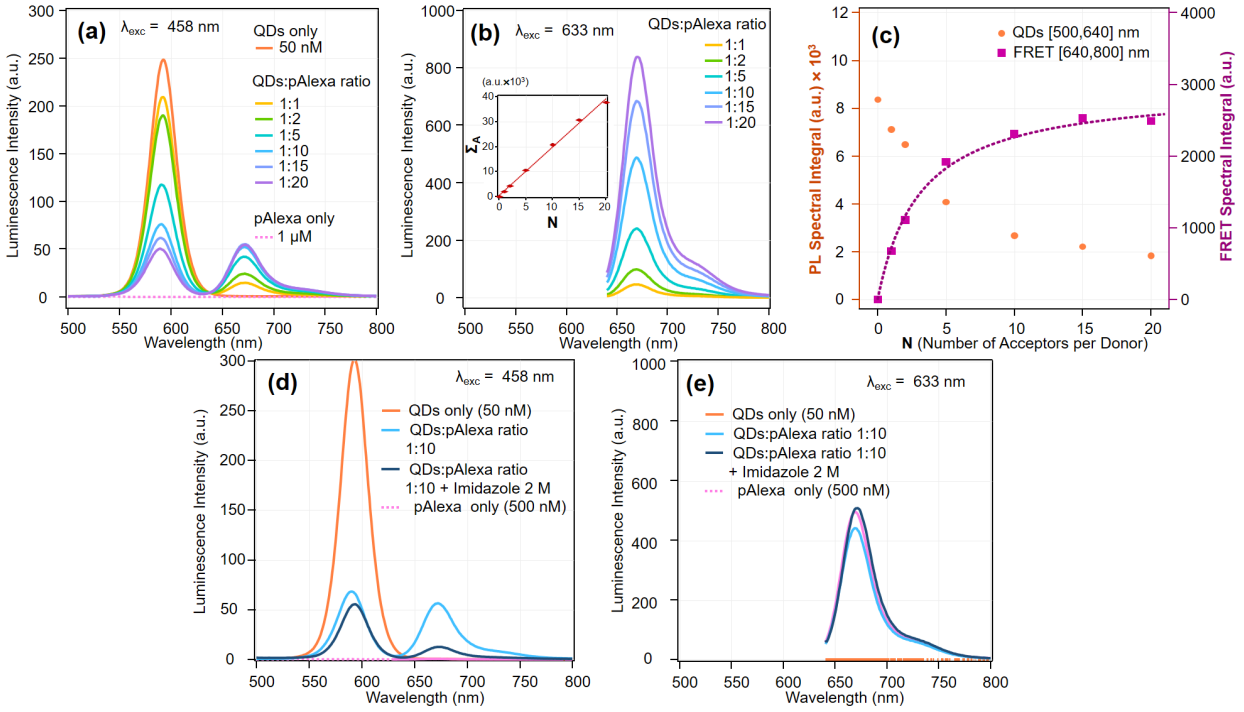

Figure 4: QDs and pAlexa solutions were mixed together to obtained the indicated ratio. (a) Photoluminescence spectrum for different QDs:pAlexa ratio recorded for an excitation wavelenght $\lambda_{exc} = 458$ nm. (b) Fluorescence spectrum for different QDs:pAlexa ratio recorded for $\lambda_{exc} = 633$ nm. The insert represents the linear variation of the spectral integral ($\Sigma = \int I(\lambda).d\lambda$) as a function of the number of acceptor N per donor. (c) QDs photoluminescence quenching and FRET signal evolution as a function of the number N of acceptors per donor. The FRET signal was fitted with a Langmuir saturation curve. (d) Effect of the addition of imidazole on the photoluminescence for 1:10 donor: acceptor concentration at $\lambda_{exc} = 458$ nm. (e) Effect of the addition of imidazole on the photoluminescence for 1:10 donor acceptor concentration at $\lambda_{exc} = 633$ nm.

the acceptor. This correlation proves that FRET process occurs between the QDs and the pAlexa (Figure 4 a). As expected, when the quantity of acceptor increases, we measure a stronger quenching of the QDs photoluminescence concomitantly to an increase of the pAlexa fluorescence. In parallel, we have also recorded the fluorescence emission of the pAlexa for an excitation wavelength at $\lambda = 633$ nm (Figure 4 b). Predictably, we measure a linear increase of the fluorescence emission with the pAlexa concentration, meaning that acceptor concentration is well controlled. In order to reach the maximum acceptor concentration that leads to the highest FRET signal, we have increased the acceptor:donor concentration ratio from 1:1 to 1:20. As a result, we have plotted the integral of the different fluorescent signals versus the number of acceptor N per donor. As shown in Figure 4 c, the quenching of the donor becomes larger while the FRET signal increases, until reaching a saturation plateau. For N higher than 10, there is no drastic changes in both signals even though acceptors were added, as proved by the fluorescence signal of the pAlexa at $\lambda = 633$ nm, which continues to grow (Figure 4 b). Therefore, there is no gain to work at concentration ratio higher than 1:10. We have fitted our results with a Langmuir saturation curve (Figure 4c):

$$\text{FRET} = \alpha \frac{K_a.N.[Donor]}{1 + K_a.N.[Donor]} \tag{1}$$

where FRET is the signal of acceptors recorded at $\lambda = 458$ nm , N is the number of acceptor per donor, [Donor] the concentration of donor, K_a the association constant and α a constant. In this experiment [Donor] = 50 nm. Thus we obtained, $K_a = (6.3 \pm 0.6).10^6$ M^{-1}. This value is coherent with the one obtained in literature, altough the previous value is higher ($10^{9,2}$ M^{-1}).[41] In fact, it is complicated to compare these two values as we are evaluating the association constant of the pAlexa molecules and not only single imidazole molecules.

In order to check the specificity of the pAlexa binding on the QDs surfaces, imidazole is added in the solution to compete with the pAlexa. We have tested different concentrations: for concentrations lower than 2 M, we did not see any effect as the FRET signal remained

the same. This means that the attachment of the pAlexa on the QDs surface is strong in comparison with common his-tag proteins purification where imidazole at a concentration of 250 μM is enough to detach proteins from Ni^{2+}-NTA resin.[42] At 2 M concentration, we obtained a high decrease of the FRET signal (Figure 4 d) due to the presence of imidazole molecules replacing the pAlexa on the QDs surface. In contrast, no changes are observed in the fluorescence of the pAlexa at λ = 633 nm (Figure 4e), meaning that the pAlexa concentration is unchanged in solution and thus pAlexa has been just removed from the QDs surface. Surprisingly, the QDs photoluminescence intensity is smaller and the emission spectrum profile is narrowed. This non-return to the initial photoluminescence level for the QDs could be explained by the presence of imidazole molecules, which play the role of new surface ligands on the QDs and therefore change their photoluminescence properties. Nevertheless, these FRET experiments conducted in solution prove that our pAlexa polymer binds specifically to the QDs with a good affinity.

FRET on micropatterned surfaces

Squared QDs micropatterns were used to demonstrate the specific interaction between the QDs monolayer and the pAlexa, thus allowing FRET. Right after the micropattern fabrication, samples were incubated with a PLL-g-PEG solution (Susos AG, PLL(20)-g[3.5]-PEG(5)) at a concentration of 0.3 mg/mL for one hour, and rinced with ultrapure water in order to passivate the glass and prevent adsorption of pAlexa elsewhere than on QDs. Then, prior to the incubation of pAlexa, the micropatterns were incubated with a histidin-RGD peptide at 1 μM in HEPES buffer for 10 min. This Histidin-RGD peptide played a dual role. Firstly, its main use is to induce adhesion on the QDs micropatterns during experiments with living cells.

Secondly, we also have observed that this peptide played also the role of a new ligand shell for the QDs as it allowed the stabilization of QDs photoluminescence when an aqueous solution is added on the top of the micropatterns. (Figure S3). This stabilization is important

to insure that there is no photobleaching of the QDs during long time illumination experiments. Finally, a solution of pAlexa at 100 μM was added for few minutes. pAlexa and histidin-RGD have a comparable size and share the same type of bond on QDs and high concentrations of the pAlexa allows for an immediate ligand exchange. The sample is then rinced with HEPES buffer in order to remove the fluorescence contribution coming from the pAlexa in solution not specifically binded to the QDs surface. Then, the micropatterns were washed 5 times with an imidazole solution (2 M) in order to specifically remove the pAlexa and incubated again for 10 min with the histidin-RGD solution previously used to be as close as possible to the initial conditions. Spectra (Figure S4) and TIRF images were recorded for each steps (Figure 5). Figure S5 shows a summary of all previously described steps.

Figure S6 shows the different spectral windows used to image the sample. Two band-pass filters were used to select the QDs or the pAlexa emission. Three successive images were recorded: I_{DD}, I_{DA} and I_{AA} (Figure 5). I_{DD} is the QDs photoluminescence, as it corresponds to the signal of donors recorded in the detection channel, for the excitation wavelength of the donors, (*i.e.* a detection restricted to λ_{det} = 570-610 nm for an excitation at λ_{exc} = 458 nm). I_{DA} signal corresponds to the targeted FRET signal, at the excitation wavelength of the donors (λ_{exc} = 458 nm) and a detection restricted to λ_{det} = 670-698 nm (pAlexa fluorescence). I_{AA} corresponds to the signal due to the resonant excitation of pAlexa, as it is recorded in the detection channel of the acceptors (λ_{det} = 670-698 nm) for the excitation wavelength of the acceptors (λ_{exc} = 633 nm). For each of the different experimental steps, the intensity scale for I_{DD}, I_{DA} and I_{AA} images is kept the same in Figure 5.

Figure 5 (Donor+Acceptor) shows that outside the patterns, there is no pAlexa. This demonstrate that the obtained pAlexa patterns reproduce faithfully the QDs patterns. The I_{AA} signal in absence of the pAlexa (Figure 5, Donor only) is at 109 $\pm$ 2 counts, which corresponds to the camera dark offset. This CMOS dark offset is a background signal which has been substracted for all following signal processing. In this "Donor only" experiment, there is a strong homogeneous emission of the QDs (19276 $\pm$ 1427 counts). On the other hand,

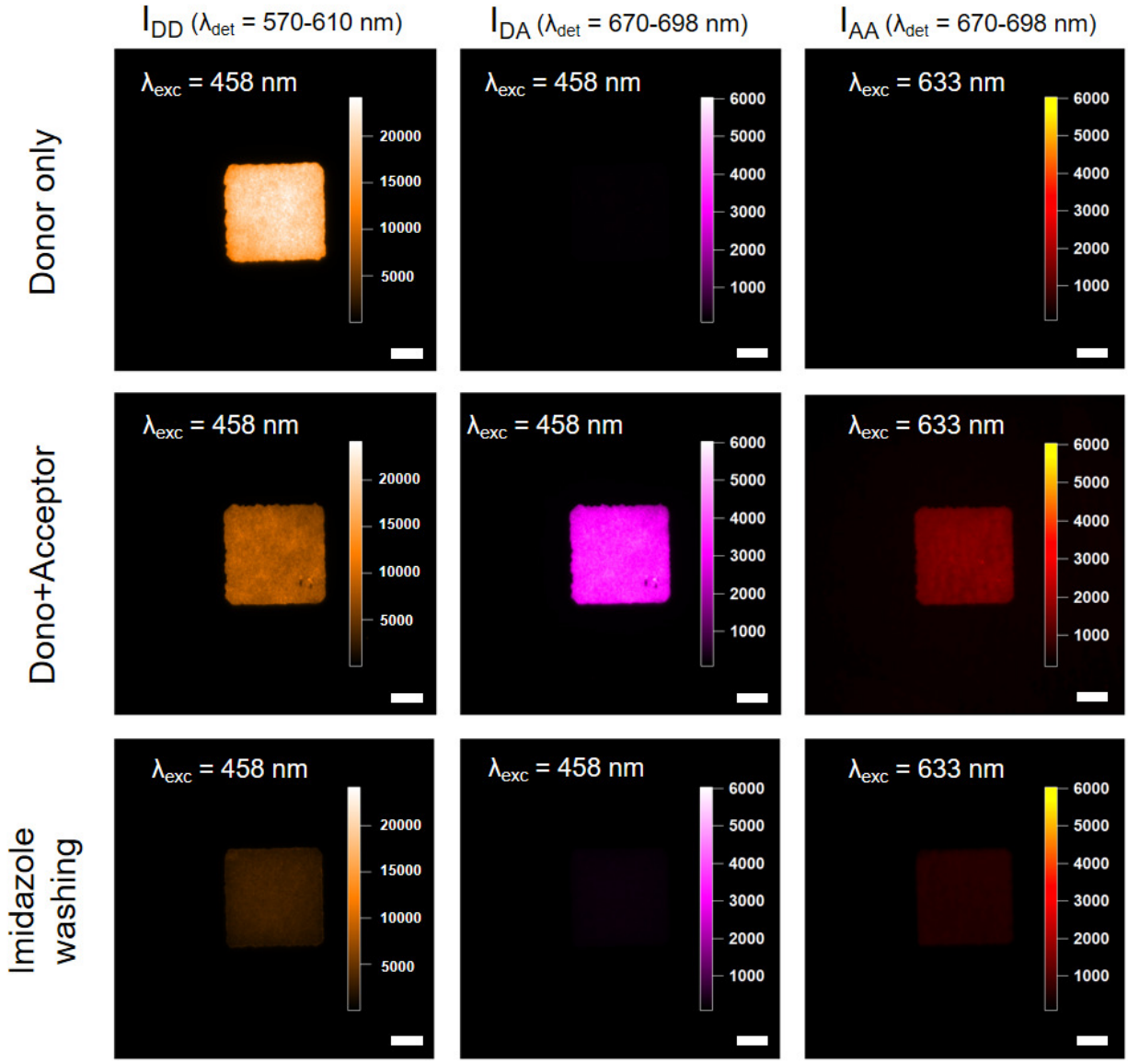

Figure 5: TIRF images of the QDs photoluminescence when QDs are alone (Donor only), when acceptor molecules are added (Donor + Acceptor) and when the surface is washed with imidazole at 2 M (Imidazole washing). I_{DD} is the QDs photoluminescence for an excitation at λ_{exc} = 458 nm and a detection window restricted to λ_{det} = 570-610 nm. Same images were recorded by changing the spectral detection window and the excitation wavelength: I_{DA} is the FRET signal obtained for an excitation at λ_{exc} = 458 nm and a detection window restricted to λ_{det} = 610-698 nm. And I_{AA} is the pAlexa fluorescence measured for an excitation waveleght at λ_{exc} = 633 nm and a detection window restricted to λ_{det} = 670-698 nm). The laser irradiance was setted at 0,9 W/cm^2 for λ_{exc} = 458 nm and at 1 W/cm^2 for λ_{exc} = 633 nm. The scale bar is 10 μm.

I_{DA} equals to 36 ± 9 counts, which corresponds to a small donor emission bleed-through in the spectral detection window of the FRET. In the "Donor + Acceptor" experiment, we clearly measure a quenching in the QDs photoluminescence on the micropatterns (Figure 5, Donor+Acceptor), as I_{DD} signal decreased to 8027 ± 759 counts. Concomitantly, the I_{DA} signal rises to 3247 ± 280 counts and the I_{AA} signal is at 1442 ± 98 counts. These different measurements prove unambiguously that FRET process occurs between the QDs and the pAlexa. We also claim that the FRET signal recorded in the I_{DA} channel (Figure 5, Donor+Acceptor) comes mainly from FRET: there is only 1% of background coming from donor bleedthrough and direct excitation of the acceptor λ_{exc} = 458 nm.

The specificity of the pAlexa binding on the QDs micropatterned was verified by rinsing the sample with an imidazole solution at 2 M, followed by incubation with the histidin-RGD peptide. As previously observed in Figure 4 c, the binding of single imidazole molecules here induced a quenching of our QDs. The I_{DD} signal goes down to 2677 ± 378 counts (Figure 5, Imidazole washing), which could also be partly explained by some losses of QDs due to the successive rinsing steps. This I_{DD} evolution corresponds to a division by ∼7 times compared the "Donor only" situation, and by ∼3 times compared to the "Donor+Acceptor" one. At the same time, the FRET signal vanished (I_{DA} = 103 ± 19 counts) due to the detachment and then the removal of most of the pAlexa (I_{AA} = 411 ± 29 counts). Here, I_{DA} is divided by ∼30 times compared to the "Donor+Acceptor" configuration, while I_{AA} is divided by a factor of 3. Some pAlexa molecules are still bounded on the QDs surfaces but their amount is too low to produce a significant FRET signal.

Finally, we investigated the possibility that our QDs micropatterning approach is suitable to observe cell adhesion. RPE-1 cells (approximatively 300 000 cells/mL) were incubated with DiD at 1 μM for 5 min in an incubator at 37 ℃. Then, 3 centrifugations at 1500 rpm were performed to remove the excess of DiD. DiD is an amphiphilic fluorescent probe (maximum emission at 647 nm) that will only stain the cell membrane (Figure 6 I_{AA}). QDs

micropatterns exhibiting disk shape were incubated with the histidin-RGD solution (1 μM) to promote cell adhesion everywhere on the sample (no PLL-g-PEG was added before). DiD stained cells were added on the sample. As we see in Figure 6 I_{DA}, FRET occurs between the QDs and the DiD when the cell membrane is in the vicinity of the QDs. At the same time and on the same area, a strong quenching in the QDs photoluminescence is recorded (Figure 6 I_{DD}). Moreover we clearly see that when the cell is outside the pattern, no FRET signal is recorded. This result demonstrates that the histidin-RGD peptide effectively allows cell adhesion and that our advanced micropatterning method is relevant for cell nano-imaging.

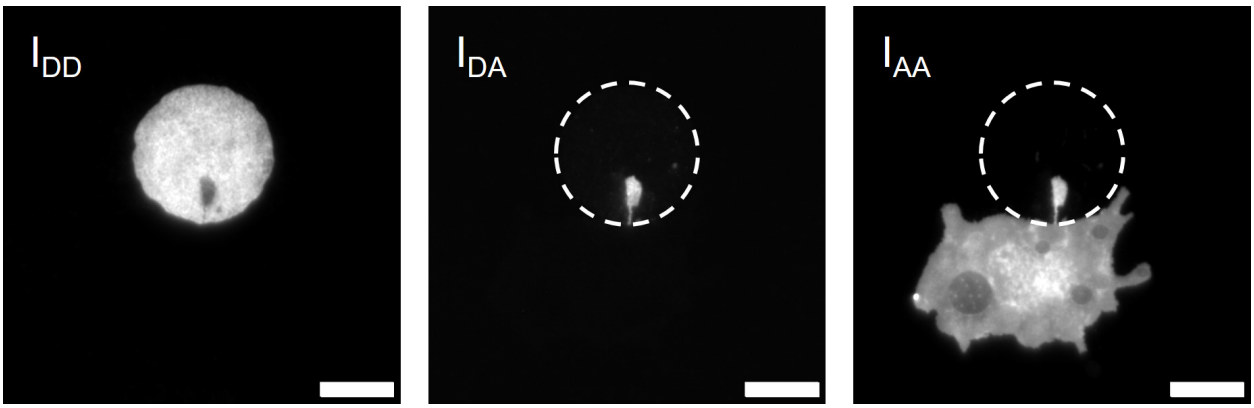

Figure 6: RPE 1 cell in adhesion in the vicinity of a circular QDs pattern. I_{DD} is the QDs photoluminescence (excitation at λ_{exc} = 458 nm, laser irradiance fixed at 0,3 W/cm^2). I_{DA} is the FRET signal occuring between the QDs and the DiD molecules present in the cell membrane (excitation λ_{exc} = 458 nm, laser irradiance = 0,3 W/cm^2). I_{AA} is the fluorescence of the DiD excited at λ_{exc} = 633 nm with an irradiance of 1 W/cm^2. The scale bar is 10 μm. The dotted line in I_{DA} and I_{AA} indicates the QDs micropattern.

Conclusion

We have developed a protocol for robust high resolution micropatterning of QDs on large scale with a free choice in the shapes. The micropatterns exhibit a dense monolayer of QDs with a typical surface density around 4000 QDs/μm^2. We have also demonstrated that any kind of molecules exhibiting imidazole tag can be specificaly attached to the micropatterned QDs. The specific and reversible nature of the binding was highlighted by measuring FRET in solution and also on the micropatterns. With our method, the bio-functionalization of the QDs micropatterns can therefore be achieved and be employed for cell nano-imaging. These promising results open a path for studying the dynamics of proteins involved in cell adhesion and migration, or for creating highly sensitive sensors measuring the appearance or disappearance of the QDs quenching and/or FRET signals.

Methods

Synthesis of QDs nanoparticles

The QDs used in this work were CdSe/CdS/CdZnS/ZnS core/multishell QDs, with emission centered between 590 and 600 nm. The synthesis of these QDs followed methodologies already reported in previous works.[43] Briefly, CdSe nanocrystals were synthesized by reaction of cadmium myristate and selenium in octadecene at 240 °C.[44] The concentration of CdSe QDs were estimated from the absorbance of the solution of CdSe core QDs using a Jasco V730 absorption spectrometer, before shell growth, as described previously.[45] The shell was grown by successive ionic layer adsorption and reaction, following previously reported protocols[46] with 3 monolayers of CdS, 3 of Cd0.5Zn0.5S and 1of ZnS. The extinction coefficient of core/shell QDs was then measured by absorption spectroscopy, assuming that the concentration of QDs remain constant during shell growth. Photoluminescence emission spectra was measured using a Cary Eclipse UV-visible fluorescence spectrometer from Agilent. Size

was measured by transmission electron microscopy. The aqueous solubilization of QDs was obtained by precipitation of 4 nmol of QDs in ethanol, followed by a centrifugation (13300 g, 5 min). After removal of the supernatants, 400 μL of mercaptopropionic acid (MPA) is mixed using a ultrasonic bath. Then, the QDs-MPA are incubated overnight at 60 ℃ and redispersed in 1 mL of chloroform. A new centrifugation is done to remove the organic ligands and then the QDs-MPA are dissolved in 1 mL of DMF, precipitated again by adding 40 mg of potassium tert-butoxide and centrifuged. The QDs precipitate is then washed with ethanol and centrifuged. The MPA-QDs are finally redispersed in 400 μL of 100 mM sodium carbonate buffer (pH = 9). The 10 μM concentration after the ligand exchange was checked by UV-Vis absorption measurements. The absorption and photoluminescence spectra (excitation wavelenght at 458 nm) of the QDs are shown in figure S7.

Micropatterning of surfaces

Photopatterning of S1813 G2 was performed using the PRIMO optical module (Alvéole) at an excitation wavelenght of $\lambda = 375$ nm controlled by the Leonardo plugin (Alvéole), mounted on a Olympus inverted microscope equipped with a $\times$10 Olympus objective. Before starting, the coverslips are cleaned with a Piranha solution (60% H_2SO_4, 40% H_2O) for 30 min and then intensively rinced with ultrapure water. The desired patterns for photoillumination were created using Inkscape (Inkscape Project) and loaded into Leonardo. The UV dose of all samples was set to 3 mJ/mm^2. The photopatterning induces a spatially controlled destruction of the S1813 G2. After photopatterning, samples are baked on hotplate at 110℃ for 10 min and then developed for 1 min under gentle agitation with MF26-A. After the developing process, samples are rinsed with ultrapure water, dried and placed in a plasma air cleaning chamber (Harrick Plasma) for 2 min to activate the surfaces for the silanization process. Next, the samples are immersed in a MPTMS solution diluted at 2 % in anhydrous toluene overnight. After rinsing with anydrous toluene, samples are immersed in a solution of QDs at 1 μM to induce their grafting to the surface through disulphiric bridges. Then, after

a rinsing step with anydrous toluene, samples are immersed in acetone solution to perform a lift-off of the S1813 G2 photoresist with 5 min of sonication. Therefore, QDs micropatterned are obtained.

Synthesis of the Histidin-RGD peptide

The GRGDSPKGAGAKG-HHHHHHH peptide was synthesized at the peptide synthesis platform at IBPS, Paris. All other chemical reagents were obtained from Sigma-Aldrich.

Synthesis of the pAlexa polymer

A modified RAFT agent was synthesized by coupling 4-cyanopentanoic acid dithiobenzoate (CADB) with 11-azido-3,6,9-trioxaundecan-1-amine ($N-TEG-NH_2$). CADB (1 mmol, 279 mg) was first mixed with dicyclocarbodiimide (2.5 mmol, 494 mg) and N-hydroxysuccinimide (2.4 mmol, 276 mg) in 10 mL anhydrous dichloromethane in an ice bath under argon. $N_3-TEG-NH_2$ (0.7 mmol, 152 mg) and triethylamine (0.8 mmol) were added and left to stir overnight and warm up to room temperature. The solution was filtered, concentrated with a rotavapor and the product was purified by chromatography on a silica column using dichloromethane and dichloromethane with methanol (2%) as eluents. The final product, CADB-N_3, was dried in a rotavapor (typical yield: 40%).

A sulfobetaine methacrylate (SPE)- block-vinylimidazole (VIM) copolymer was synthesized using $CADB-N_3$ as a RAFT agent following a protocol adapted from Tasso *et al.*[38] Briefly, SPE (0.55 g, 2 mmol) was dissolved in 40 mL sodium acetate buffer (0.1 M, pH 4.5) and mixed with CADB-N_3 (0.2 mmol, 100 mg) dissolved in 2mL tetrahydrofuran. V50 (0.04 mmol, 12 mg) was added, and the solution was deoxygenated by bubbling argon for 20 min. The solution was then heated at 70°C for 2h under argon. The obtained SPE-CADB-N_3 macro-RAFT was precipitated in acetone twice and dried under vacuum. The number of

SPE unit per polymer was estimated at 30 by 1H NMR. The second block was polymerized by dissolving SPE−CADB−N_3 (36 μmol, 300 mg) and vinylimidazole (360 μmol, 34 mg) in 0.5 mL water (100 mM sodium chloride). Azobisisobutyronitrile (AIBN, 40 μmol, 6.6 mg) was dissolved in 4.5 mL acetic acid. Both solutions were mixed together, deoxygenated by argon bubbling and reacted at 70 ℃ for 6 hours under argon. The obtained p(SPE−b−VIM)−N_3 polymer was precipitated twice with acetone and dried under vacuum. On average, 7 VIM units per polymer chain as estimated by 1H NMR.

p(SPE−b−VIM)−N_3 (0.75 μmol, 6.2 mg) was dissolved in 100 μL HEPES buffer (10 mM, pH 7.4; 150 mM NaCl), mixed with AlexaFluor647-DBCO (0.9 μmol, 1 mg in 20 μL dimethylsulfoxyde) and reacted for 24h at room temperature. The resulting p(SPE-b-VIM)-AF647 polymer was purified by three rounds of ultrafiltration (Vivaspin, 3 kDa), precipitated with acetone, and resuspended in 200 μL HEPES buffer. The final concentration was estimated from the absorbance of AF647 at 652 nm, using an extinction coefficient of 239,000 $M^{-1}cm^{-1}$. The absorption and fluorescence spectra (excitation wavelenght at $\lambda = 633$ nm) of the pAlexa are shown in figure S7.

Spectra measurements in solution

We use a Cary Eclipse UV-visible fluorescence spectrometer from Agilent to perform all measurements in solution. The speed scan was setted at 120 nm/min. The intervall between each measured points was fixed at 1 nm and the averaging time for each point is fixed at 0.5 s.

Optical set-up, image acquisition and spectra measurement on micropatterns

Our set-up was extensively described in a previous paper.[15] Briefly, observations are performed on a Zeiss inverted microscope in TIRF illumination configuration with a ×63 Zeiss

objective (NA = 1.46). The microscope is enclosed in an hermetic chamber to allow observations at 37℃. Two laser beams are implemented: one at 458 nm for QDs excitation and another one at 633 nm for direct excitation of acceptor molecules. The illumination irradiance was tuned by using neutral density. Band pass filters were used to observe the QDs emission or the acceptor emission are purchased from Semrock (FF01-590/20-25 and FF01-684/24-25). The camera used in all experiments was an Orca Flash 4.0 Hamamatsu. Images in this work are the average of 25 successive acquisitions (t = 500 ms). A USB2000+ spectrometer from Ocean Optics was also added to record spectrum. Spectral data of the micropatterns in (Supporting informations) are the averaged of 10 patterns measurements, each of them having been subject to 25 successive acquisitions (t = 1 s).

Cell culture and DiD staining

RPE1 hTERT-immortalized retinal pigment epithelial cells were grown in DMEM/F-12 Glutamax (Gibco 31331) supplemented with 10% of fetal bovine serum (Gibco, Thermo Fisher Scientific, Waltham, MA) and 1% of antibiotics/antifungal mixture (penicillin, streptomycin, amphotericin B; Lonza) in a humidified atmosphere at 37 ℃ with 5% CO_2. For TIRF measurements, cells were observed in a nonfluorescent culture medium at λ = 458 nm. We used DMEMgfp-2 medium (Dulbecco's modified Eagle's medium; Evrogen, Moscow, Russia) supplemented with L-glutamine at 2 mM (Gibco), HEPES buffer at 20 mM (Gibco), and only 1% of fetal bovine serum.

For plasma membrane labeling, we used the well-known DiD probe (1,1'-dioctadecyl - 3,3,3',3'-tetramethylindodicarbocyanine, 4-Chlorobenzenesulfonate salt DilC18 (5); Invitrogen-Thermo Fisher Scientific). Membrane labeling was performed as previously described.[15]

Supporting Information Available

- Figure S1: Relation between the photoluminescence of surfaces and the surface density of the QDs monolayer, for different acquisition parameters.
- Figure S2: scheme of the pAlexa polymer structure.
- Figure S3: Evolution of the QDs micropatterns photoluminescence under continuous illumination during 10 min, for different interfaces.
- Figure S4: Spectra recorded on the QDs micropatterns.
- Figure S5: Scheme of the different steps performed on the QDs micropatterns FRET experiment
- Figure S6: Spectral characterization of the detection channels used for imaging.
- Figure S7: Absorption spectra for QDs and pAlexa, QDs photoluminescence spectrum (λ_{ext} = 458 nm) and pAlexa fluorescence spectrum (λ_{ext}= 633 nm)

Acknowledgement

We thank C. Piesse (Peptide Synthesis Platform at IBPS, Paris) for the peptide synthesis. This project received financial support from the CNRS through the MITI interdisciplinary programs, from the Conseil Départemental de l'Aube (CD10) of the Région Grand Est and from the European Regional Development Fund (ERDF) 2014/2020.

References

(1) Hines, M. A.; Guyot-Sionnest, P. Synthesis and Characterization of Strongly Luminescing ZnS-Capped CdSe Nanocrystals. *The Journal of Physical Chemistry* **1996**, *100*, 468–471.

(2) Shirasaki, Y.; Supran, G. J.; Bawendi, M. G.; Bulović, V. Emergence of colloidal quantum-dot light-emitting technologies. *Nature Photonics* **2013**, *7*, 13–23.

(3) Lim, J.; Jeong, B. G.; Park, M.; Kim, J. K.; Pietryga, J. M.; Park, Y.-S.; Klimov, V. I.; Lee, C.; Lee, D. C.; Bae, W. K. Influence of Shell Thickness on the Performance of Light-Emitting Devices Based on CdSe/Zn1-XCdXS Core/Shell Heterostructured Quantum Dots. *Advanced Materials* **2014**, *26*, 8034–8040.

(4) Zhang, C.-Y.; Yeh, H.-C.; Kuroki, M. T.; Wang, T.-H. Single-quantum-dot-based DNA nanosensor. *Nature Materials* **2005**, *4*, 826–831.

(5) Mattoussi, H.; Palui, G.; Na, H. B. Luminescent quantum dots as platforms for probing in vitro and in vivo biological processes. *Advanced Drug Delivery Reviews* **2012**, *64*, 138–166.

(6) Khalid, W.; Helou, M. E.; Murböck, T.; Yue, Z.; Montenegro, J.-M.; Schubert, K.; Göbel, G.; Lisdat, F.; Witte, G.; Parak, W. J. Immobilization of Quantum Dots *via* Conjugated Self-Assembled Monolayers and Their Application as a Light-Controlled Sensor for the Detection of Hydrogen Peroxide. *ACS Nano* **2011**, *5*, 9870–9876.

(7) Pattantyus-Abraham, A. G.; Qiao, H.; Shan, J.; Abel, K. A.; Wang, T.-S.; van Veggel, F. C. J. M.; Young, J. F. Site-Selective Optical Coupling of PbSe Nanocrystals to Si-Based Photonic Crystal Microcavities. *Nano Letters* **2009**, *9*, 2849–2854.

(8) Omari, A.; Geiregat, P.; Thourhout, D. V.; Hens, Z. Light absorption in hybrid silicon-on-insulator/quantum dot waveguides. *Optics Express* **2013**, *21*, 23272.

(9) Kirkwood, N.; Singh, B.; Mulvaney, P. Enhancing Quantum Dot LED Efficiency by Tuning Electron Mobility in the ZnO Electron Transport Layer. *Advanced Materials Interfaces* **2016**, *3*, 1600868.

(10) Azzellino, G.; Freyria, F. S.; Nasilowski, M.; Bawendi, M. G.; Bulović, V. Micron-Scale Patterning of High Quantum Yield Quantum Dot LEDs. *Advanced Materials Technologies* **2019**, *4*, 1800727.

(11) Riachy, L.; El Arawi, D.; Jaffiol, R.; Vézy, C. Nanometer-Scale Resolution Achieved with Nonradiative Excitation. *ACS Photonics* **2018**, *5*, 2217–2224.

(12) Chan, W. C.; Maxwell, D. J.; Gao, X.; Bailey, R. E.; Han, M.; Nie, S. Luminescent quantum dots for multiplexed biological detection and imaging. *Current Opinion in Biotechnology* **2002**, *13*, 40–46.

(13) Winckler, P.; Jaffiol, R.; Plain, J.; Royer, P. Nonradiative Excitation Fluorescence: Probing Volumes Down to the Attoliter Range. *Journal of Physical Chemistry Letters* **2010**, *1*, 2451–2454.

(14) Spiess, M.; Hernandez-Varas, P.; Oddone, A.; Olofsson, H.; Blom, H.; Waithe, D.; Lock, J. G.; Lakadamyali, M.; Strömblad, S. Active and inactive β1 integrins segregate into distinct nanoclusters in focal adhesions. *Journal of Cell Biology* **2018**, *217*, 1929–1940.

(15) El Arawi, D.; Vézy, C.; Déturche, R.; Lehmann, M.; Kessler, H.; Dontenwill, M.; Jaffiol, R. Advanced quantification for single-cell adhesion by variable-angle TIRF nanoscopy. *Biophysical Reports* **2021**, *1*, 100021.

(16) Kanchanawong, P.; Shtengel, G.; Pasapera, A. M.; Ramko, E. B.; Davidson, M. W.; Hess, H. F.; Waterman, C. M. Nanoscale architecture of integrin-based cell adhesions. *Nature* **2010**, *468*, 580–584.

(17) Zelená, A.; Isbaner, S.; Ruhlandt, D.; Chizhik, A.; Cassini, C.; Klymchenko, A. S.; Enderlein, J.; Chizhik, A.; Köster, S. Time-resolved MIET measurements of blood platelet spreading and adhesion. *Nanoscale* **2020**, *12*, 21306–21315.

(18) Engler, A. J.; Griffin, M. A.; Sen, S.; Bonnemann, C. G.; Sweeney, H. L.; Discher, D. E. Myotubes differentiate optimally on substrates with tissue-like stiffness. *Journal of Cell Biology* **2004**, *166*, 877–887.

(19) Théry, M. Micropatterning as a tool to decipher cell morphogenesis and functions. *Journal of Cell Science* **2010**, *123*, 4201–4213.

(20) Théry, M.; Racine, V.; Piel, M.; Pépin, A.; Dimitrov, A.; Chen, Y.; Sibarita, J.-B.; Bornens, M. Anisotropy of cell adhesive microenvironment governs cell internal organization and orientation of polarity. *Proceedings of the National Academy of Sciences* **2006**, *103*, 19771–19776.

(21) Sapsford, K. E.; Medintz, I. L.; Golden, J. P.; Deschamps, J. R.; Uyeda, H. T.; Mattoussi, H. Surface-Immobilized Self-Assembled Protein-Based Quantum Dot Nanoassemblies. *Langmuir* **2004**, *20*, 7720–7728.

(22) Yang, J.; Lee, M.; Park, S. Y.; Park, M.; Kim, J.; Sitapure, N.; Hahm, D.; Rhee, S.; Lee, D.; Jo, H.; Jo, Y. H.; Lim, J.; Kim, J.; Shin, T. J.; Lee, D. C.; Kwak, K.; Kwon, J. S.; Kim, B.; Bae, W. K.; Kang, M. S. Nondestructive Photopatterning of Heavy-Metal-Free Quantum Dots. *Advanced Materials* **2022**, *34*, 2205504.

(23) Hahm, D.; Lim, J.; Kim, H.; Shin, J.-W.; Hwang, S.; Rhee, S.; Chang, J. H.; Yang, J.; Lim, C. H.; Jo, H.; Choi, B.; Cho, N. S.; Park, Y.-S.; Lee, D. C.; Hwang, E.; Chung, S.; Kang, C.-m.; Kang, M. S.; Bae, W. K. Direct patterning of colloidal quantum dots with adaptable dual-ligand surface. *Nature Nanotechnology* **2022**, *17*, 952–958.

(24) Yang, J.; Hahm, D.; Kim, K.; Rhee, S.; Lee, M.; Kim, S.; Chang, J. H.; Park, H. W.; Lim, J.; Lee, M.; Kim, H.; Bang, J.; Ahn, H.; Cho, J. H.; Kwak, J.; Kim, B.; Lee, C.; Bae, W. K.; Kang, M. S. High-resolution patterning of colloidal quantum dots via non-destructive, light-driven ligand crosslinking. *Nature Communications* **2020**, *11*, 2874.

(25) Na, Y. J.; Park, S. J.; Lee, S. W.; Kim, J. S. Photolithographic process for the patterning of quantum dots. *Ultramicroscopy* **2008**, *108*, 1297–1301.

(26) Rabouw, F. T.; Frimmer, M.; Mohtashami, A.; Koenderink, A. F. Nanoscale lithographic positioning of fluorescing quantum dot nanocrystals on planar samples. *Optical Materials* **2013**, *35*, 1342–1347.

(27) Dieleman, C. D.; Ding, W.; Wu, L.; Thakur, N.; Bespalov, I.; Daiber, B.; Ekinci, Y.; Castellanos, S.; Ehrler, B. Universal direct patterning of colloidal quantum dots by (extreme) ultraviolet and electron beam lithography. *Nanoscale* **2020**, *12*, 11306–11316.

(28) Cho, H.; Pan, J.-A.; Wu, H.; Lan, X.; Coropceanu, I.; Wang, Y.; Cho, W.; Hill, E. A.; Anderson, J. S.; Talapin, D. V. Direct Optical Patterning of Quantum Dot Light-Emitting Diodes via In Situ Ligand Exchange. *Advanced Materials* **2020**, *32*, 2003805.

(29) Keum, H.; Jiang, Y.; Park, J. K.; Flanagan, J. C.; Shim, M.; Kim, S. Photoresist Contact Patterning of Quantum Dot Films. *ACS Nano* **2018**, *12*, 10024–10031, PMID: 30247027.

(30) Bäumle, M.; Stamou, D.; Segura, J.-M.; Hovius, R.; Vogel, H. Highly Fluorescent Streptavidin-Coated CdSe Nanoparticles: Preparation in Water, Characterization, and Micropatterning. *Langmuir* **2004**, *20*, 3828–3831.

(31) Choi, M. K.; Yang, J.; Kang, K.; Kim, D. C.; Choi, C.; Park, C.; Kim, S. J.; Chae, S. I.; Kim, T.-H.; Kim, J. H.; Hyeon, T.; Kim, D.-H. Wearable red–green–blue quantum dot light-emitting diode array using high-resolution intaglio transfer printing. *Nature Communications* **2015**, *6*.

(32) Wood, V.; Panzer, M. J.; Chen, J.; Bradley, M. S.; Halpert, J. E.; Bawendi, M. G.; Bulovíc, V. Inkjet-Printed Quantum Dot-Polymer Composites for Full-Color AC-Driven Displays. *Advanced Materials* **2009**, *21*, 2151–2155.

(33) Xie, W.; Gomes, R.; Aubert, T.; Bisschop, S.; Zhu, Y.; Hens, Z.; Brainis, E.; Van Thourhout, D. Nanoscale and Single-Dot Patterning of Colloidal Quantum Dots. *Nano Letters* **2015**, *15*, 7481–7487, PMID: 26455513.

(34) Zhang, M.; Hu, B.; Meng, L.; Bian, R.; Wang, S.; Wang, Y.; Liu, H.; Jiang, L. Ultrasmooth Quantum Dot Micropatterns by a Facile Controllable Liquid-Transfer Approach: Low-Cost Fabrication of High-Performance QLED. *Journal of the American Chemical Society* **2018**, *140*, 8690–8695, PMID: 29894177.

(35) Kim, B. H.; Onses, M. S.; Lim, J. B.; Nam, S.; Oh, N.; Kim, H.; Yu, K. J.; Lee, J. W.; Kim, J.-H.; Kang, S.-K.; Lee, C. H.; Lee, J.; Shin, J. H.; Kim, N. H.; Leal, C.; Shim, M.; Rogers, J. A. High-Resolution Patterns of Quantum Dots Formed by Electrohydrodynamic Jet Printing for Light-Emitting Diodes. *Nano Letters* **2015**, *15*, 969–973, PMID: 25584701.

(36) Wang, Y.; Pan, J.-A.; Wu, H.; Talapin, D. V. Direct Wavelength-Selective Optical and Electron-Beam Lithography of Functional Inorganic Nanomaterials. *ACS Nano* **2019**, *13*, 13917–13931.

(37) Strale, P.-O.; Azioune, A.; Bugnicourt, G.; Lecomte, Y.; Chahid, M.; Studer, V. Multiprotein Printing by Light-Induced Molecular Adsorption. *Advanced Materials* **2015**, *28*, 2024–2029.

(38) Tasso, M.; Giovanelli, E.; Zala, D.; Bouccara, S.; Fragola, A.; Hanafi, M.; Lenkei, Z.; Pons, T.; Lequeux, N. Sulfobetaine–Vinylimidazole Block Copolymers: A Robust Quantum Dot Surface Chemistry Expanding Bioimaging's Horizons. *ACS Nano* **2015**, *9*, 11479–11489.

(39) Liu, W.; Greytak, A. B.; Lee, J.; Wong, C. R.; Park, J.; Marshall, L. F.; Jiang, W.; Curtin, P. N.; Ting, A. Y.; Nocera, D. G.; Fukumura, D.; Jain, R. K.; Bawendi, M. G.

Compact Biocompatible Quantum Dots via RAFT-Mediated Synthesis of Imidazole-Based Random Copolymer Ligand. *Journal of the American Chemical Society* **2010**, *132*, 472–483.

(40) Kikuchi, M.; Terayama, Y.; Ishikawa, T.; Hoshino, T.; Kobayashi, M.; Ohta, N.; Jinnai, H.; Takahara, A. Salt Dependence of the Chain Stiffness and Excluded-Volume Strength for the Polymethacrylate-Type Sulfopropylbetaine in Aqueous NaCl Solutions. *Macromolecules* **2015**, *48*, 7194–7204.

(41) Sundberg, R. J.; Martin, R. B. Interactions of histidine and other imidazole derivatives with transition metal ions in chemical and biological systems. *Chemical Reviews* **1974**, *74*, 471–517.

(42) Bornhorst, J. A.; Falke, J. J. *Methods in Enzymology*; Elsevier, 2000; pp 245–254.

(43) Trapiella-Alfonso, L.; Pons, T.; Lequeux, N.; Leleu, L.; Grimaldi, J.; Tasso, M.; Oujagir, E.; Seguin, J.; d'Orlyé, F.; Girard, C.; Doan, B.-T.; Varenne, A. Clickable-Zwitterionic Copolymer Capped-Quantum Dots for in Vivo Fluorescence Tumor Imaging. *ACS Applied Materials & Interfaces* **2018**, *10*, 17107–17116.

(44) Yang, Y. A.; Wu, H.; Williams, K. R.; Cao, Y. C. Synthesis of CdSe and CdTe Nanocrystals without Precursor Injection. *Angewandte Chemie International Edition* **2005**, *44*, 6712–6715.

(45) Leatherdale, C. A.; Woo, W.-K.; Mikulec, F. V.; Bawendi, M. G. On the Absorption Cross Section of CdSe Nanocrystal Quantum Dots. *The Journal of Physical Chemistry B* **2002**, *106*, 7619–7622.

(46) Li, J. J.; Wang, Y. A.; Guo, W.; Keay, J. C.; Mishima, T. D.; Johnson, M. B.; Peng, X. Large-Scale Synthesis of Nearly Monodisperse CdSe/CdS Core/Shell Nanocrystals Using Air-Stable Reagents via Successive Ion Layer Adsorption and Reaction. *Journal of the American Chemical Society* **2003**, *125*, 12567–12575.

TOC Graphic

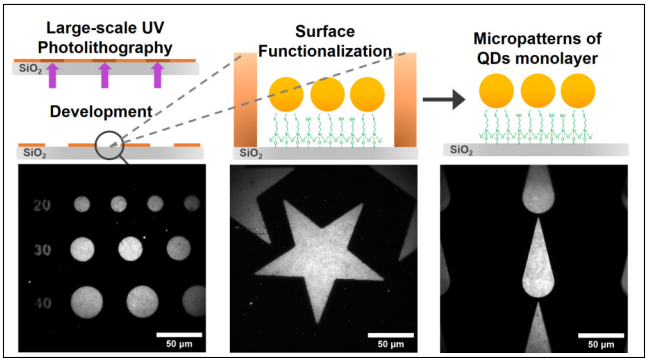
Large-scale UV
Photolithography
SiO2
Development
SiO2
Surface
Functionalization
SiO2
Micropatterns of
QDs monolayer
SiO2
20
30
40
50 μm
50 μm
50 μm